

# Phase-controlled elastic, inelastic, and coalescent collisions of two-dimensional flat-top solitons

M. O. D. Alotaibi<sup>1,\*</sup>, Y. O. A. Abughnheim<sup>2</sup>, L. Al Sakkaf<sup>3</sup>, and U. Al Khawaja<sup>2,4</sup>

<sup>1</sup>*Department of Physics, College of Science, Kuwait University,*

*Sabah Al Salem University City, P.O. Box 5969, Safat 13060, Shadadiya, Kuwait,*

<sup>2</sup>*Department of Physics, School of Science, The University of Jordan, Amman 11942, Jordan,*

<sup>3</sup>*Department of Applied Sciences, College of Engineering,*

*Abu Dhabi University, Al-Ain 59911, United Arab Emirates,*

<sup>4</sup>*Department of Physics, United Arab Emirates University,*

*P.O. Box 15551, Al-Ain, United Arab Emirates.\**

We investigate elastic, inelastic, and coalescent collisions between two-dimensional flat-top solitons supported by the cubic–quintic nonlinear Schrödinger equation. Numerical simulations reveal distinct collision regimes ranging from nearly elastic scattering to strongly inelastic interactions leading to long-lived merged states. We demonstrate that the transition between these regimes is primarily controlled by the relative phase of the solitons at the collision point, with out-of-phase collisions suppressing overlap and in-phase collisions promoting strong interaction. Kinetic-energy diagnostics are introduced to quantitatively characterize collision outcomes and to identify phase- and separation-dependent windows of elasticity. To interpret the observed dynamics, we extract effective phase-dependent interaction potentials from collision trajectories, providing a mechanical picture of attraction and repulsion between flat-top solitons. The stability of merged states formed after strongly inelastic collisions is explained by their lower energetic cost, arising from interfacial energetics, where a balance between internal pressure and edge tension plays a central role. A variational analysis based on direct energy minimization supports this picture by revealing robust energetic minima associated with stationary two-dimensional flat-top solitons.

## I. INTRODUCTION

Solitons are localized nonlinear excitations arising from a balance between dispersion and nonlinearity and are distinguished by their robustness under propagation and interaction [1–8]. In integrable one-dimensional models, such as the cubic nonlinear Schrödinger equation (NLSE), solitons undergo perfectly elastic collisions: after interaction, each soliton recovers its original shape, velocity, and amplitude, up to a phase shift [9, 10]. When integrability is broken, either through competing nonlinearities or by increasing the dimensionality, soliton interactions may become inelastic, allowing for radiation emission, excitation of internal modes, deformation, or fusion[11].

Flat-top solitons (FTSs) represent a particularly rich class of nonintegrable localized states. They arise, for instance, in systems with competing self-focusing and self-defocusing nonlinearities, most commonly cubic and quintic terms, and are characterized by an extended, nearly uniform bulk density bounded by relatively sharp edges [12–22]

This structure leads to liquid-like properties in FTSs, including an effectively incompressible interior and a finite ‘surface’ tension associated with their interfaces. Such states have been predicted and observed in a variety of physical settings, including nonlinear optical media and ultracold atomic systems [23]. The collision dynamics of one-dimensional FTSs has been studied in detail [24, 25].

In particular, earlier work demonstrated that the transition between elastic and inelastic collisions is primarily controlled by the *relative phase at the collision point* [25]. Out-of-phase collisions significantly suppress overlap and lead to nearly elastic scattering, whereas in-phase collisions promote strong overlap, radiation emission, and, in some cases, permanent merger. These regimes were quantitatively characterized using kinetic-energy diagnostics and further interpreted in terms of effective interaction forces, establishing a coherent picture in which interference, nonintegrability, and energetics jointly govern the collision outcome.

Despite this progress, comparatively little is known about collisions of *two-dimensional* FTSs. Extending collision studies to higher dimensions is not a trivial generalization. In two dimensions, flat-top solitons possess extended interfaces whose curvature and energetic cost play a central role in their dynamics, and additional channels for transverse deformation and radiation become available. As a result, inelastic collisions may lead not only to transient distortion but also to long-lived merged states, whose stability cannot be understood solely on the basis of phase interference.

In this work we investigate collisions of two-dimensional FTSs within the cubic–quintic nonlinear Schrödinger equation. Using numerical simulations, we demonstrate that, as in one dimension, the relative phase at the collision point remains the dominant control parameter determining whether collisions are elastic or inelastic. However, the two-dimensional geometry enriches the inelastic dynamics through transverse deformation, enhanced radiation, and the emergence of stable coalesced states. To

\* Contact author: majed.alotaibi@ku.edu.kw

quantitatively distinguish collision regimes, we introduce kinetic-energy diagnostics that reveal clear separation- and phase-dependent windows of elasticity and inelasticity.

Beyond the dynamical characterization, we develop two complementary interpretations of the observed behavior. First, we extract effective phase-dependent interaction forces and potentials directly from collision trajectories, providing a mechanical picture of attraction for in-phase solitons and repulsion for out-of-phase solitons. Second, we connect the outcome of strongly inelastic collisions to the energetic structure of stationary two-dimensional FTSs. By combining interfacial energetics and a Young–Laplace–type balance [23], in which the bulk pressure pushing outward is balanced by edge tension pulling inward, with a variational description based on direct energy minimization, we show that merged states correspond to stable energetic minima and are not merely transient outcomes of the collision. Together, these results establish a unified framework for understanding elastic, inelastic, and coalescent collisions of two-dimensional FTSs, linking phase interference, effective forces, and energetic stability in a higher-dimensional setting.

This article proceeds as follows. In Sec. II, we introduce the two-dimensional cubic–quintic nonlinear Schrödinger equation and summarize its conserved quantities. Section III describes the numerical construction of stationary two-dimensional FTSs and the initialization of two-soliton configurations via imaginary-time propagation (ITP). Direct real-time simulations of FTS collisions are presented in Sec. IV, with emphasis on the role of the relative phase at the collision point. In Sec. V, kinetic-energy diagnostics are introduced to quantitatively distinguish elastic, nearly elastic, and inelastic collision regimes, and their dependence on initial separation and phase is analyzed. Effective interaction forces and potentials extracted from collision dynamics are discussed in Sec. V.C, providing a mechanical interpretation of phase-controlled attraction and repulsion. The formation and stability of long-lived merged states following strongly inelastic collisions are examined in Sec. VI, where interfacial energetics and a Young–Laplace–type balance are used to explain their persistence. The paper concludes in Sec. VII with a summary of the main results and an outlook for future work.

## II. THEORETICAL MODEL

We study the two-dimensional cubic–quintic nonlinear Schrödinger equation

$$i\psi_t + g_1(\psi_{xx} + \psi_{yy}) + g_2|\psi|^2\psi + g_3|\psi|^4\psi = 0, \quad (1)$$

where  $\psi(x, y, t)$  denotes the complex field envelope. The coefficient  $g_1$  controls the dispersive term, while  $g_2 > 0$  and  $g_3 < 0$  represent cubic self-focusing and quintic self-defocusing nonlinearities, respectively. The balance be-

tween dispersion and nonlinear response enables localization, while the competition between cubic self-focusing and quintic self-defocusing nonlinearities gives rise to flat-top soliton profiles.

Equation (1) is nonintegrable, and as a consequence soliton interactions are not constrained to be perfectly elastic. Collisions may therefore involve radiation emission, waveform deformation, or permanent merger, depending on the interaction parameters. This intrinsic nonintegrability underlies the inelastic collision dynamics examined in the following sections. Stationary FTSs are sought in the form

$$\psi(x, y, t) = u(x, y) e^{-i\mu t}, \quad (2)$$

which leads to the nonlinear elliptic equation

$$\mu u + g_1(u_{xx} + u_{yy}) + g_2u^3 + g_3u^5 = 0. \quad (3)$$

In the flat-top regime, the solution  $u(x, y)$  exhibits an approximately constant density in the bulk, with the nonlinear terms nearly balancing,

$$g_2u^2 + g_3u^4 \approx -\mu, \quad (4)$$

while gradient contributions become significant only near the soliton boundary. Because Eq. (3) does not admit closed-form localized solutions in two dimensions, stationary states are obtained numerically, as described in Sec. III. The conserved quantities associated with Eq. (1) are the norm,

$$N = \int_{-\infty}^{\infty} \int_{-\infty}^{\infty} |\psi|^2 dx dy, \quad (5)$$

the momentum,

$$P = (P_x, P_y), \quad P_{x,y} = \int_{-\infty}^{\infty} \int_{-\infty}^{\infty} \text{Im}(\psi^* \psi_{x,y}) dx dy, \quad (6)$$

and the total energy,

$$E = \int_{-\infty}^{\infty} \int_{-\infty}^{\infty} \left[ g_1(|\psi_x|^2 + |\psi_y|^2) - \frac{1}{2}g_2|\psi|^4 - \frac{1}{3}g_3|\psi|^6 \right] dx dy. \quad (7)$$

These conserved quantities provide the energetic and dynamical framework used to characterize collision outcomes in the subsequent analysis.

## III. STATIONARY FLAT-TOP SOLITONS AND INITIALIZATION

Stationary two-dimensional FTSs are obtained numerically by ITP of Eq. (1) using a split-step Fourier method. Throughout this work we set  $g_1 = 1/2$  and fix the nonlinear coefficients to  $g_2 = 4$  and  $g_3 = -4$ , and impose a

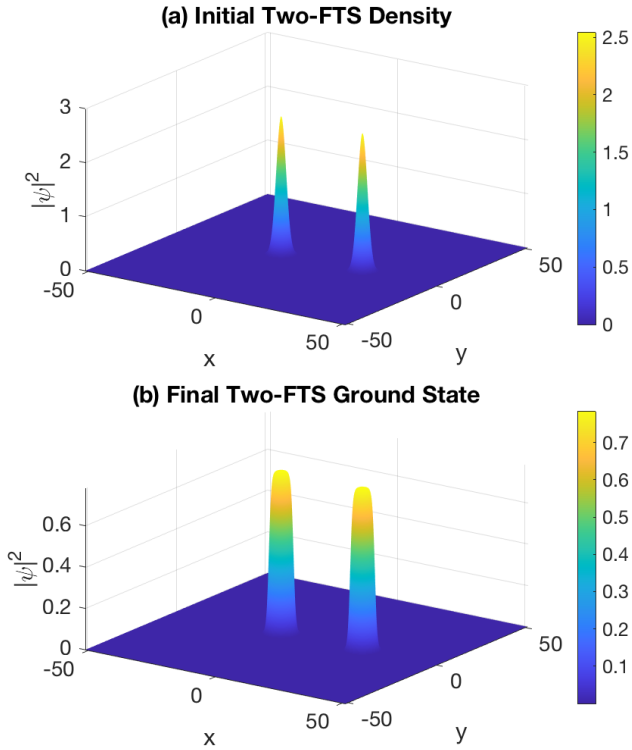


FIG. 1: Initial and final density surfaces used in the numerical setup. (a) Initial two-Gaussian seed of width  $w = 10$ , centered at  $(x_1, y_1) = (-10, 0)$  and  $(x_2, y_2) = (22, 0)$ . (b) Stationary two-FTS state obtained after ITP.

target norm  $N = 80$ . The ITP evolution converges to the minimum-energy state at fixed norm, yielding radially symmetric FTSs. To construct a stationary two-soliton configuration, the initial field is taken as a superposition of two broad Gaussian seeds of common width  $w = 10$ , namely

$$\psi(x, y, 0) = \sum_{j=1}^2 \exp \left[ -\frac{(x - x_j)^2 + (y - y_j)^2}{w^2} \right], \quad (8)$$

where  $(x_1, y_1) = (-10, 0)$  and  $(x_2, y_2) = (22, 0)$ . The field is normalized to the target norm and evolved in imaginary time until convergence. The relaxed state obtained after ITP represents the two-flat-top-soliton ground state. Figure 1 illustrates a representative ITP relaxation from the initial two-Gaussian seed to the stationary two-FTS configuration, while Fig. 2 shows a central density slice comparing the initial and final states.

#### IV. COLLISION DYNAMICS

In this section we examine collisions between two-dimensional FTSs with an emphasis on the role of the *relative phase* at the collision point. All simulations are performed using a Fourier split-step method on a  $1024 \times 1024$  grid with spatial steps  $dx = dy = 0.1$  and time step

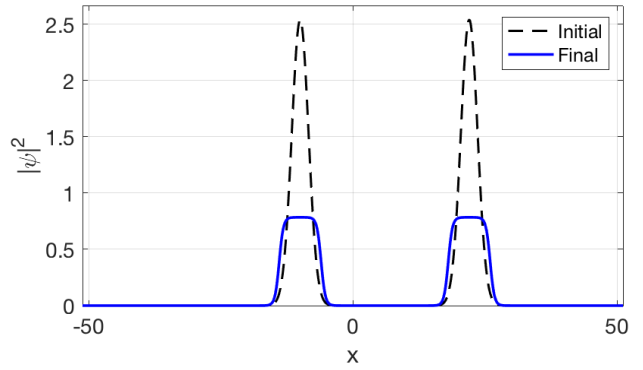


FIG. 2: Central slice comparison of the initial two-Gaussian seed and the stationary two-FTS state produced by ITP, for the same parameters as in Fig. 1.

$dt = 5 \times 10^{-4}$ , under periodic boundary conditions. To isolate the phase-controlled interaction mechanism, we keep all numerical and physical parameters fixed and vary only the initial horizontal separation between the solitons, which determines the accumulated relative phase at impact.

Both simulations use identical velocity assignments, with the first soliton initially at rest ( $V_{1x} = V_{1y} = 0$ ) and the second soliton moving toward it with velocity  $V_{2x} = -0.3$  and  $V_{2y} = 0$ , so that the collision occurs along a straight line. The motion of the second soliton is generated by applying an initial phase imprinting (kick) to its stationary profile within the two-soliton configuration obtained by ITP. The resulting initial condition for the real-time evolution is taken as

$$\psi(x, y, 0) = \sum_{j=1}^2 u_j(x - x_j, y - y_j) \exp[i(V_{jx}x + V_{jy}y)], \quad (9)$$

where  $u_j(x, y)$  denotes the stationary flat-top soliton, and  $(V_{jx}, V_{jy})$  specify the imposed velocities of the individual solitons, as described above. The only change between the two collision scenarios is the initial location of the second soliton:

$$(x_2, y_2) = \begin{cases} (30, 0), & \text{Case (a): elastic scattering,} \\ (15, 0), & \text{Case (b): inelastic scattering.} \end{cases}$$

To connect the two-dimensional collision dynamics shown in Fig. 3 with the underlying interaction mechanism, we extract one-dimensional slices along  $y = 0$  of both the density and the phase. These slices reveal the degree of soliton overlap and the relative phase at the collision point. Figures 4 and 5 show the corresponding density  $|\psi(x, t)|^2$  and phase evolution.

In the *elastic* case  $(x_2, y_2) = (30, 0)$ , the solitons reach the interaction region with a phase difference close to  $\pi$ , as evidenced by the phase evolution shown in Fig. 4, which suppresses overlap and energy exchange. In the *inelastic* case  $(x_2, y_2) = (15, 0)$ , the solitons are nearly in

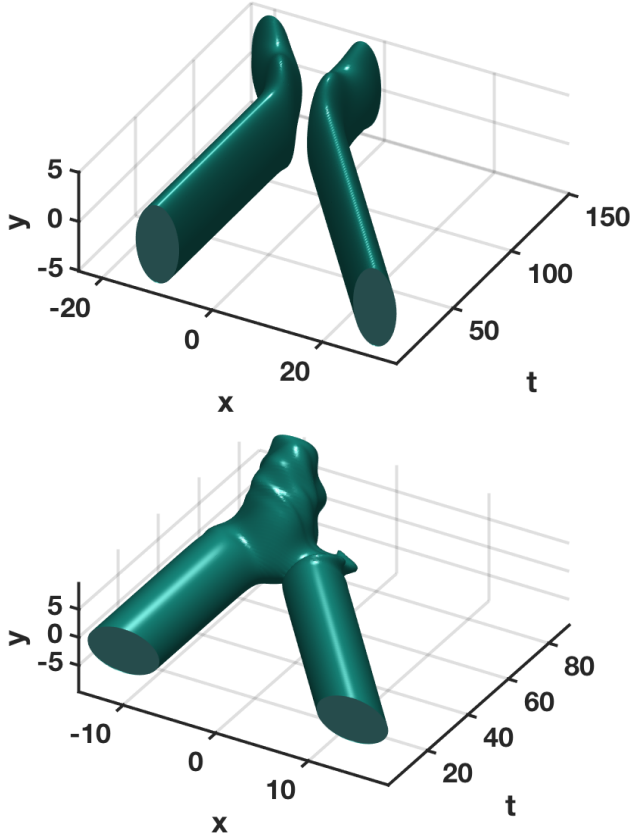


FIG. 3: Comparison of two collision scenarios obtained with identical parameters, differing only in the initial  $x$ -position of the second soliton. (a) Elastic scattering for  $(x_2, y_2) = (30, 0)$ . (b) Inelastic scattering for  $(x_2, y_2) = (15, 0)$ . The qualitative difference arises from the relative phase at the collision point.

phase at impact, as shown in Fig. 5, overlap strongly, and emit radiation accompanied by long-lasting deformation. Since all parameters are identical except for the initial separation, these results demonstrate that the *relative phase at impact* is the dominant control parameter for elastic versus inelastic collisions.

## V. KINETIC-ENERGY DIAGNOSTICS OF ELASTIC AND INELASTIC COLLISIONS

To quantitatively distinguish elastic from inelastic collision outcomes, we monitor the kinetic energy of the system before and after the collision. In an elastic collision, the kinetic energy is conserved, whereas in an inelastic collision a finite fraction of kinetic energy is irreversibly transferred to radiation and internal excitations. Accordingly, we introduce the change in kinetic energy,

$$\Delta KE = KE_{\text{after}} - KE_{\text{before}}, \quad (10)$$

as a global diagnostic of collision elasticity. Values of  $\Delta KE$  close to zero indicate nearly elastic collisions, while

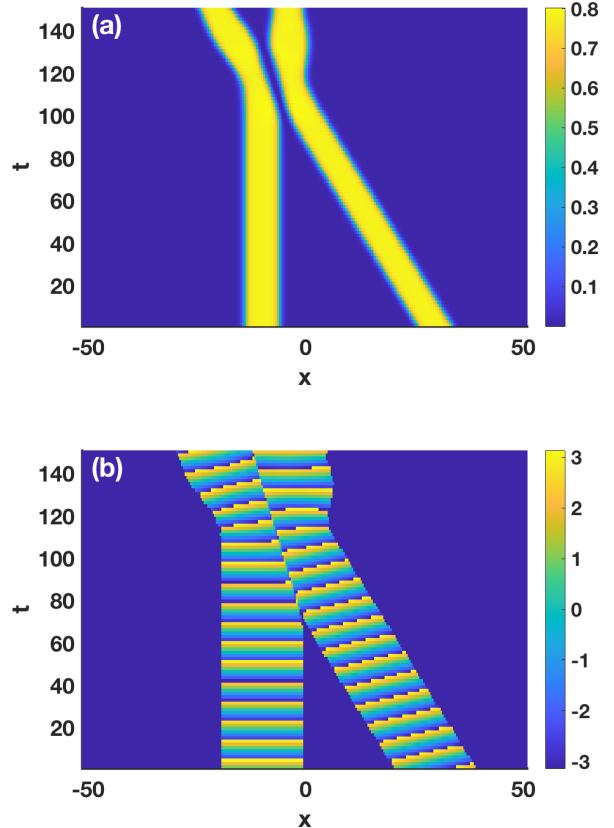


FIG. 4: Density and phase evolution along  $y = 0$  for the elastic collision. (a) Density shows negligible overlap. (b) Phase shows a relative phase close to  $\pi$  at the collision point.

larger deviations signal inelastic behavior.

### V.A. Separation-dependent kinetic-energy diagnostics

We first examine how the collision elasticity varies with the initial separation  $\Delta x = x_2 - x_1$  between the two FTSs, while keeping all other parameters fixed. In all cases the first soliton is held fixed at  $x_1 = -10$ , as in the initialization described in Sec. III, and the separation is varied by changing the position  $x_2$  of the second soliton. For each value of  $\Delta x$ , a stationary two-soliton initial state is prepared by ITP, followed by real-time evolution with identical collision velocities. The change in kinetic energy  $\Delta KE$ , defined in Eq. (10), is used here as a quantitative diagnostic of the collision outcome.

Figure 6 shows that a clear low- $\Delta KE$  window appears over an intermediate range of  $\Delta x$ , indicating nearly elastic collisions, while both smaller and larger separations lead to significantly larger  $\Delta KE$  and strongly inelastic behavior. This dependence on  $\Delta x$  reflects the role of the

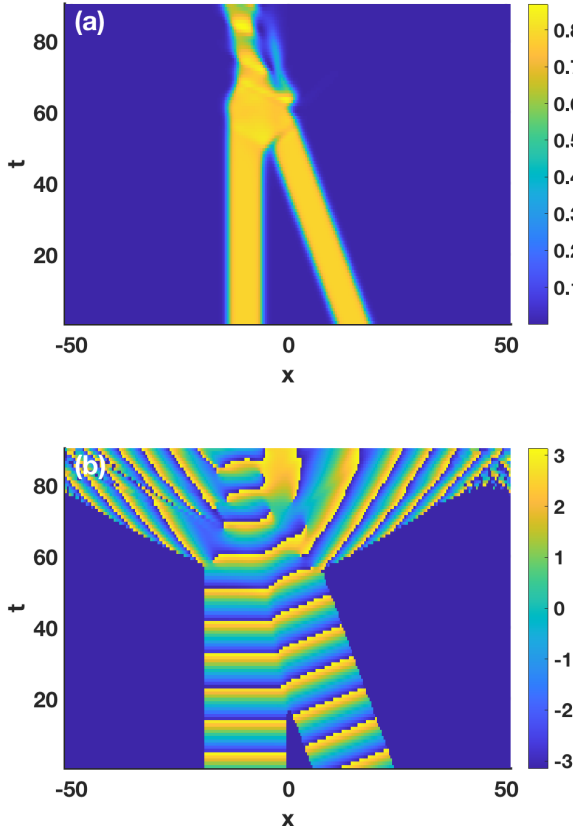


FIG. 5: Density and phase evolution along  $y = 0$  for the **inelastic** collision. (a) Density shows strong overlap. (b) Phase shows a relative phase close to 0 at the collision point, leading to deformation and radiation.

accumulated relative phase at the collision point. Varying the initial separation effectively tunes the phase difference at impact, leading to alternating elastic and inelastic collision windows.

### V.B. Phase-dependent kinetic-energy diagnostics

In an alternative approach, we examine the dependence of the collision elasticity on the *initially imposed* phase difference  $\Delta\phi$  between the two FTSSs, while keeping all other physical and numerical parameters fixed. In particular, the soliton velocities, initial separation, norm, and nonlinear coefficients are identical for all runs in this subsection. The parameter  $\Delta\phi$  is introduced by imprinting a uniform phase shift on one of the solitons in the stationary two-soliton initial state prior to real-time evolution.

We emphasize that  $\Delta\phi$  denotes the relative phase at the initial time  $t = 0$ . During propagation, each soliton acquires additional phase, so the phase difference at the collision point is generally different from the initially imposed value. Nevertheless, since all other parameters are

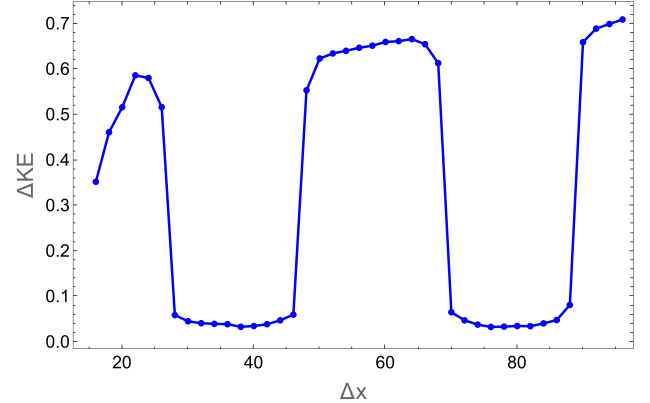


FIG. 6: Change in kinetic energy  $\Delta KE$  as a function of the initial separation  $\Delta x = x_2 - x_1$  between two FTSSs. A clear low- $\Delta KE$  window is observed over an intermediate range of  $\Delta x$ , indicating nearly elastic collisions, while larger values of  $\Delta KE$  correspond to increasingly inelastic behavior.

held fixed, the phase difference at impact is a deterministic function of  $\Delta\phi$ , allowing the collision dynamics to be parametrized in terms of the initial phase difference. For each value of  $\Delta\phi$ , the system is evolved in real time using the same collision protocol, and the collision outcome is quantified by computing the change in kinetic energy  $\Delta KE$ , defined in Eq. (10), before and after the collision.

Figure 7 shows the dependence of  $\Delta KE$  on the initial phase difference  $\Delta\phi$ . The collision outcome exhibits a periodic dependence on  $\Delta\phi$ . Initial phases that lead to out-of-phase configurations at the collision point produce minimal kinetic-energy change, with the two FTSSs emerging as distinct entities. In contrast, initial phases that result in approximately in-phase collisions lead to a substantial increase in  $\Delta KE$  and strongly inelastic behavior, in which the two solitons merge into a single flat-top structure.

This clear dependence on phase shows that the elasticity of collisions between two-dimensional FTSSs is controlled by the relative phase at the moment of impact. When combined with the separation-dependent results in Sec. V.A, this also shows that the alternating elastic and inelastic collision windows, observed as the initial separation is varied, arise from the phase accumulated by the solitons during their propagation before collision.

In addition, we note that when all parameters are fixed and only the collision velocity is varied, the collision outcome is still determined by the relative phase at impact, as in the separation- and phase-dependent analyses. However, increasing the velocity leads to increasingly hard collisions, and although elastic and inelastic outcomes remain clearly distinguishable, the rapid onset of strong deformation and breakup prevents the emergence of a simple periodic dependence of  $\Delta KE$  on velocity.

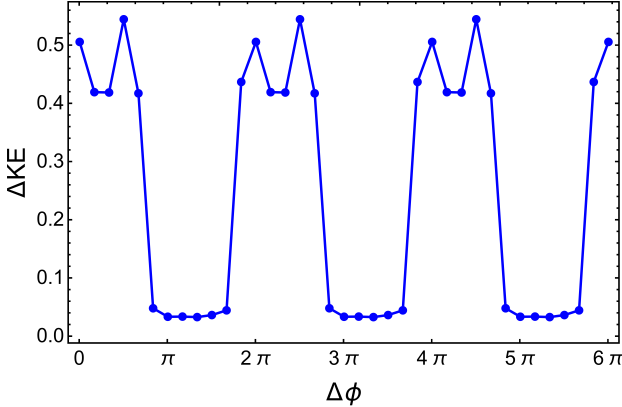


FIG. 7: Change in kinetic energy  $\Delta KE$  as a function of the *initially imposed* relative phase difference  $\Delta\phi$  between two FTSs. The parameter  $\Delta\phi$  labels the phase difference at  $t = 0$ ; the relative phase at the collision point is modified during propagation by dynamical phase accumulation. Nearly elastic collisions, characterized by  $\Delta KE \approx 0$ , occur for initial phases leading to out-of-phase configurations at impact, in which the two solitons remain distinct after collision. In contrast, large values of  $\Delta KE$  correspond to strongly inelastic collisions, where the solitons merge into a single flat-top structure. The periodic dependence on  $\Delta\phi$  highlights the dominant role of phase in controlling the collision outcome.

### V.C. Effective interaction forces obtained from collision dynamics

The collision dynamics presented above demonstrate that the relative phase at the collision point controls whether two FTSs repel, overlap, or merge. To provide a complementary mechanical interpretation of this behavior, we extract an effective interaction force between the solitons directly from their real-time collision dynamics.

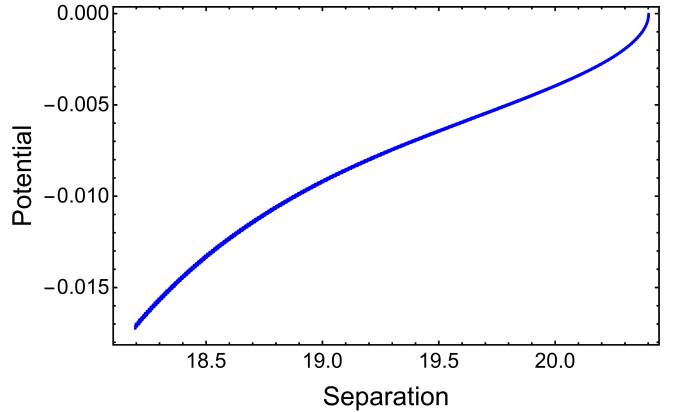
To this end, we consider an initial configuration in which two flat-top solitons are placed side by side at rest. We focus on whether the interaction is effectively attractive or repulsive as a function of the relative phase. In particular, we track the time-dependent separation  $s(t)$  between the soliton centers of mass. The center-of-mass position of each soliton is defined through the density-weighted coordinate

$$\mathbf{R}_j(t) = \frac{\int \mathbf{r} |\psi_j(\mathbf{r}, t)|^2 d^2r}{\int |\psi_j(\mathbf{r}, t)|^2 d^2r}, \quad j = 1, 2, \quad (11)$$

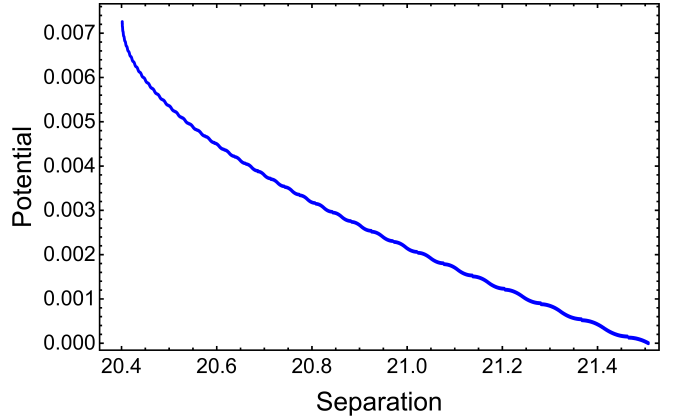
so that the instantaneous separation is given by  $s(t) = |\mathbf{R}_2(t) - \mathbf{R}_1(t)|$ . From the measured trajectory, an effective equation of motion may be written in the form

$$M \ddot{s} = F(s), \quad (12)$$

where  $M = m/2$  is an effective reduced mass. The corresponding effective interaction potential is obtained by



(a) In-phase interaction ( $\chi = 0$ ): attractive effective potential.



(b) Out-of-phase interaction ( $\chi = \pi$ ): repulsive effective potential.

FIG. 8: Effective interaction potentials  $V(s)$  extracted from real-time collision dynamics of two FTSs. The potentials are shifted such that  $V(\infty) = 0$ .

integration,

$$V(s) = - \int_s^\infty F(s') ds', \quad (13)$$

with the normalization  $V(\infty) = 0$  imposed numerically.

The resulting effective interaction potentials extracted from the collision trajectories are shown in Fig. 8. In-phase collisions,  $\chi = 0$ , where  $\chi$  is the phase difference at collision, lead to an attractive effective potential, as shown in Fig. 8(a), while out-of-phase collisions,  $\chi = \pi$ , produce a repulsive effective potential, Fig. 8(b). Consistent with Fig. 8, in-phase collisions lead to strong overlap and, in many cases, soliton merger, whereas out-of-phase collisions suppress overlap and favor elastic scattering.

In the strongly inelastic regime, the attractive effective interaction explains *how* the two solitons are driven into strong overlap, but it does not by itself explain *why* the resulting merged object remains stable instead of rapidly fragmenting or dispersing. To address this point, we next examine the energetic cost associated with the soliton interface. This leads naturally to an interpretation based

on interfacial energetics and a Young–Laplace–type balance, whereby the bulk pressure inside the flat-top structure is balanced by a finite interfacial line tension at its curved boundary. Such a balance provides a physical mechanism for the stabilization of merged FTSs formed after strongly inelastic collisions.

## VI. COALESCENCE AND LONG-LIVED MERGED STATES

Some inelastic collisions lead to long-lived merged or permanently coalesced states, in which the two FTSs do not re-separate after impact. While a complete dynamical theory of permanent coalescence is beyond the scope of the present collision-focused work, the persistence of merged states can be understood quantitatively in terms of the interfacial (edge) energetics of two-dimensional FTSs, together with a variational characterization of their bulk structure. These elements provide a consistent energetic framework for interpreting why strong overlap during inelastic collisions relaxes toward a stable merged configuration rather than leading to disintegration.

### VI.A. Interfacial energetics and Young–Laplace balance

We summarize the energetic ingredients underlying the stabilization mechanism, following the approach of Ref. [23]. For stationary states  $\psi = u(r)e^{-i\mu t}$  at fixed chemical potential  $\mu$ , stability is governed by the minimization of the grand potential,

$$\Omega[u] = E[u] - \mu N[u], \quad (14)$$

rather than by minimization of the energy  $E$  alone. Substituting Eqs. (5) and (7) into Eq. (14) yields

$$\begin{aligned} \Omega[\psi] = \iint \left[ \frac{1}{2} (|\psi_x|^2 + |\psi_y|^2) - \frac{g_2}{2} |\psi|^4 - \frac{g_3}{3} |\psi|^6 \right. \\ \left. - \mu |\psi|^2 \right] dx dy. \end{aligned} \quad (15)$$

In two dimensions at zero temperature, the pressure is defined as the derivative of the grand potential with respect to the transverse area,  $p = -(\frac{\partial \Omega}{\partial S})_\mu$ , where  $S$  is the two-dimensional area of the system and the derivative is taken at fixed chemical potential  $\mu$ . For stationary radially symmetric states, this definition leads to the local pressure

$$p(r) = -\frac{1}{2} u_r^2 + \frac{g_2}{2} u^4 + \frac{g_3}{3} u^6 + \mu u^2. \quad (16)$$

For FTSs,  $p(r)$  is positive and nearly constant in the bulk ( $p_c > 0$ ), while it becomes negative within a narrow interfacial region where gradient contributions dominate, cf.

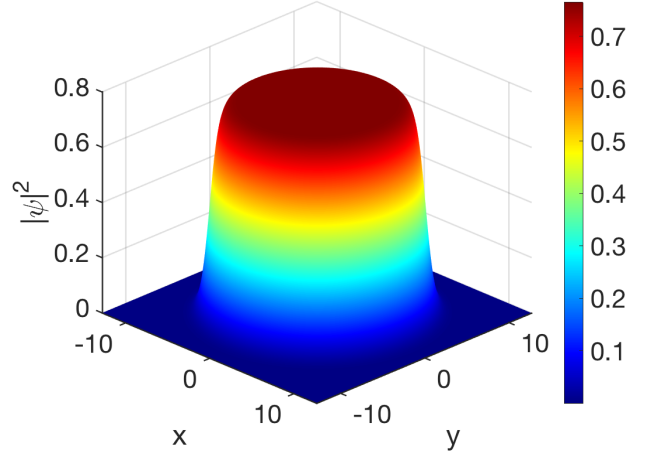


FIG. 9: Stationary single two-dimensional flat-top soliton obtained by ITP of Eq. (1) with cubic–quintic nonlinearities  $g_2 = 4$  and  $g_3 = -4$ , and norm  $N = 200$ .

The computation converges to a ground state with chemical potential  $\mu \simeq -0.717$  and total energy  $E \simeq -136.24$ . The soliton exhibits a nearly uniform bulk density with peak amplitude  $|\psi|_{\max} \simeq 0.875$  and characteristic width FWHM  $\simeq 18.18$ . This stationary state serves as the reference configuration used to compute the radial pressure profile and line tension shown in Fig. 10.

Fig. 10. The corresponding line tension (surface tension in three dimensions) is obtained as  $\sigma = -\frac{1}{R} \int_R^\infty r p(r) dr$ , where  $R$  is the soliton radius. Minimization of  $\Omega$  with respect to  $R$  yields a two-dimensional Young–Laplace–type balance,  $p_c \simeq \frac{\sigma}{R}$ .

The stationary single flat-top soliton shown in Fig. 9 is obtained from an independent ITP run of Eq. (1), using the same nonlinear parameters as in the collision simulations ( $g_2 = 4$ ,  $g_3 = -4$ ), but without a second soliton present. For this reference state, the ITP converges to a ground state characterized by  $N = 200$ ,  $E = -136.24$ , and  $\mu = -0.7171$ . The corresponding density profile exhibits a nearly uniform bulk interior with a full width at half maximum FWHM  $\simeq 18.18$  and a peak amplitude  $|\psi|_{\max} \simeq 0.875$ .

Using this stationary reference configuration, the radial pressure profile  $p(r)$  shown in Fig. 10 is computed from the radially averaged density. From this profile, the bulk pressure is found to be  $p_c \simeq 2.46 \times 10^{-2}$ . The soliton radius, defined as the location where the radial density drops most steeply, is  $R \simeq 9.07$ . The corresponding grand potential is  $\Omega \simeq 7.18$ , yielding a line tension  $\sigma \simeq 0.238$ . These values satisfy the Young–Laplace relation to good accuracy, with  $\sigma/R \simeq 2.62 \times 10^{-2}$ , consistent with the bulk pressure extracted directly from  $p(r)$ .

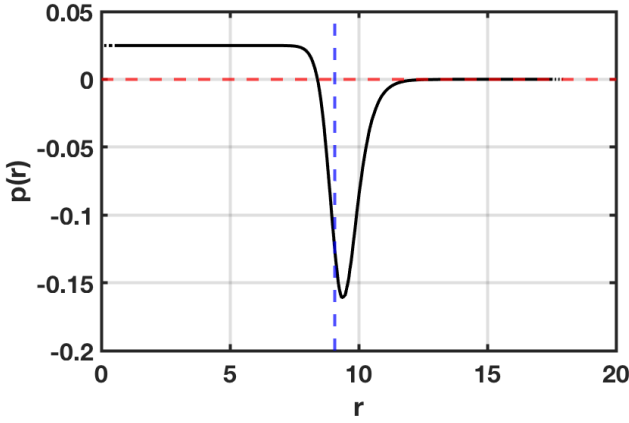


FIG. 10: Radial pressure profile  $p(r)$  computed from the stationary single flat-top soliton shown in Fig. 9. The pressure is positive and nearly constant in the bulk ( $p_c$ ), becomes negative in a narrow interfacial (edge) region dominated by gradients, and approaches zero outside. The dashed line marks the interface radius  $R$ , defined as the radius where the density drops most steeply and used to compute the line tension  $\sigma$ .

### VI.B. Variational energetic stability of merged states

A second quantitative element is that the stationary FTS used in our simulations possess a robust energetic structure that can be captured by a compact variational baseline. Single-soliton ground states are radially symmetric and can therefore be parameterized by a super-Gaussian ansatz,

$$\psi(r) = A \exp\left[-\frac{1}{2} \left(\frac{r}{w}\right)^{2m}\right], \quad (17)$$

with fixed norm  $N$ . Evaluating the conserved energy functional on this profile yields

$$E(w, m) = \frac{g_1 m^2 N}{\Gamma(1/m) w^2} - \frac{g_2 m N^2}{2\pi 2^{1/m} \Gamma(1/m) w^2} - \frac{g_3 m^2 N^3}{3\pi^2 3^{1/m} [\Gamma(1/m)]^2 w^4}, \quad (18)$$

where the amplitude follows from norm conservation,

$$A = \sqrt{\frac{Nm}{\pi\Gamma(1/m)}} \frac{1}{w}. \quad (19)$$

The variational parameters  $(w, m)$  are determined by direct minimization of  $E(w, m)$ ,

$$\frac{\partial E}{\partial w} = 0, \quad \frac{\partial E}{\partial m} = 0. \quad (20)$$

For representative parameters  $g_1 = 1/2$ ,  $g_2 = 4$ ,  $g_3 = -4$ , and  $N = 100$ , this procedure yields

$$w_0 = 6.643, \quad m_0 = 4.227, \quad A_0 = 0.8906. \quad (21)$$

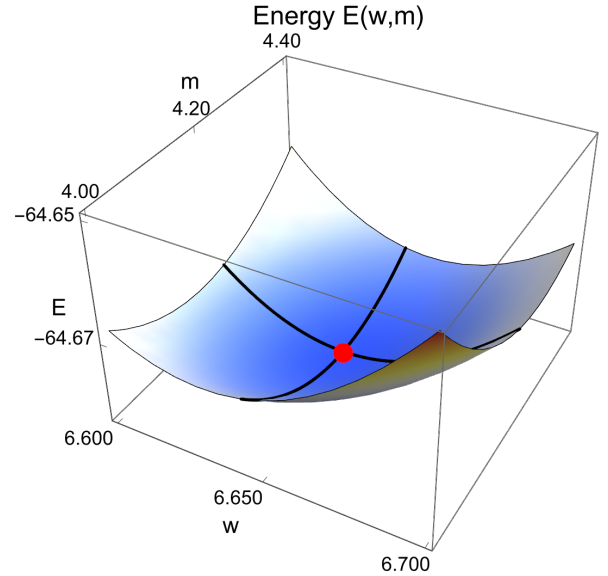


FIG. 11: Energy surface  $E(w, m)$  obtained by evaluating the variational energy functional [Eq. (18)] for the super-Gaussian ansatz at fixed norm. The numerical parameters used are  $g_1 = 0.5$ ,  $g_2 = 4$ ,  $g_3 = -4$ , and  $N = 100$ . The marked minimum at  $(w_0, m_0) = (6.643, 4.227)$  corresponds to a variationally stable flat-top soliton, as discussed in the text.

The stationary point  $(w_0, m_0)$  corresponds to a local minimum of the energy surface. This is confirmed by the positive definiteness of the Hessian matrix evaluated at this point,

$$H = \begin{pmatrix} \frac{\partial^2 E}{\partial w^2} & \frac{\partial^2 E}{\partial w \partial m} \\ \frac{\partial^2 E}{\partial w \partial m} & \frac{\partial^2 E}{\partial m^2} \end{pmatrix} = \begin{pmatrix} 11.73 & -0.666 \\ -0.666 & 0.547 \end{pmatrix}, \quad (22)$$

with  $\frac{\partial^2 E}{\partial w^2} > 0$ ,  $\frac{\partial^2 E}{\partial m^2} > 0$ , and  $\det(H) = 5.97 > 0$ . The corresponding energy surface and its minimum are shown in Fig. 11.

The existence of this local energetic minimum explains why, once strong overlap occurs during an inelastic collision, the system relaxes toward a stable merged configuration rather than fragmenting or dispersing. As a result, the two FTSs lose their individual soliton identities and coalesce into a single, long-lived structure. In this sense, coalescence represents a natural outcome of the combined bulk incompressibility and interfacial energetic cost inherent to two-dimensional FTSs.

We quantify the accuracy of the variational energy minimum by comparing the variational energy evaluated at the optimal parameters  $(w_0, m_0)$  with exact stationary ground states obtained independently by ITP of Eq. (1) at fixed norm. For each value of the norm  $N$ , the ITP procedure converges to the minimum-energy stationary solution, which serves as a numerical reference.

TABLE I: Comparison of variational and exact stationary energies for different norms  $N$ . For each  $N$ ,  $E_{\text{ITP}}$  is obtained from ITP, while  $E_{\text{VA}}$  is evaluated at the corresponding variational energy minimum. The relative deviation  $\epsilon$  is defined in the text.

$N$	$E_{\text{ITP}}$	$E_{\text{VA}}$	$\epsilon$
100	-65.1408	-64.6915	$6.90 \times 10^{-3}$
140	-93.4132	-92.8441	$6.09 \times 10^{-3}$
160	-107.6437	-107.0200	$5.80 \times 10^{-3}$
180	-121.9216	-121.2470	$5.53 \times 10^{-3}$
200	-136.2398	-135.5150	$5.32 \times 10^{-3}$

For a representative case with  $N = 100$ , the exact ground-state energy obtained by ITP is  $E_{\text{ITP}} = -65.1408$ . The energy-minimized variational ansatz (EVA), with optimal parameters  $w = 6.643$  and  $m = 4.227$ , yields  $E_{\text{VA}} = -64.6915$ , corresponding to a relative deviation  $\epsilon = |E_{\text{VA}} - E_{\text{ITP}}|/|E_{\text{ITP}}| \simeq 6.9 \times 10^{-3}$ . This level of agreement confirms that direct energy minimization provides an accurate energetic description of stationary two-dimensional FTSs.

Table I extends this comparison to a broader range of norms. The persistence of small relative deviations across increasing  $N$  demonstrates that the variational minimum represents a robust energetic feature rather than a fine-tuned solution. This robustness supports the interpretation that, once strong overlap is induced during an inelastic collision, the system relaxes toward a stable merged configuration associated with this energetic basin rather than fragmenting or dispersing.

To further support this energetic interpretation, we performed a direct numerical comparison between the energy of the coalesced flat-top soliton formed after an inelastic collision and the combined energy of the two initially separated solitons before collision. Starting from a stationary ITP configuration of two well-separated flat-top solitons with equal norms  $N_L = N_R = 100$ , we obtain a total pre-collision energy  $E_{\text{two}} = E_L + E_R = -130.26$ . After a strongly inelastic collision, we calculate the energy of the bound post-collision state, excluding the emitted radiation. This coalesced core has a slightly reduced norm  $N_{\text{core}} = 196.09$ , due to radiative losses during the collision, and a lower energy  $E_{\text{core}} = -130.88$ . Crucially, the inequality  $E_{\text{core}} < E_{\text{two}}$  holds, with a difference  $\Delta E = -0.62$ , demonstrating that the merged configuration is energetically favored over two separated flat-top solitons. This explains why the solitons remain coalesced after collision. In contrast to the integrable one-dimensional cubic NLSE, where the energy of two solitons is simply the sum of their individual energies and a merged state can split back into two solitons without any energetic penalty, the cubic-quintic model considered here is nonintegrable, and radiation losses allow the system to relax into a lower-energy bound state. This numerical energy comparison therefore confirms that coalescence in two-dimensional flat-top solitons is energet-

ically driven rather than a transient dynamical effect.

## VII. CONCLUSIONS

We have investigated elastic, inelastic, and coalescent collisions of two-dimensional FTSs supported by the cubic-quintic nonlinear Schrödinger equation. Several main conclusions emerge from this study.

First, we find that despite the intrinsic nonintegrability of the two-dimensional system, flat-top soliton collisions can exhibit well-defined regimes of nearly elastic and inelastic scattering. As in earlier studies of one-dimensional flat-top soliton collisions, the transition between elastic and inelastic regimes is primarily controlled by the relative phase of the solitons at the collision point. Out-of-phase collisions suppress overlap and radiation emission, leading to nearly elastic scattering, whereas in-phase collisions promote strong overlap and energy redistribution, resulting in inelastic behavior. Kinetic-energy diagnostics provide a clear and quantitative characterization of this phase-controlled transition.

Second, we have shown that the dependence of collision outcomes on initial separation and imposed initial phase arises from deterministic phase accumulation during propagation. By varying the initial separation, one effectively tunes the relative phase at impact, leading to alternating windows of elastic and inelastic scattering. This phase-controlled structure persists in two dimensions despite the presence of transverse degrees of freedom and additional radiation channels, underscoring the central role of phase interference in organizing flat-top soliton collision dynamics.

Third, a subset of strongly inelastic collisions leads to long-lived merged or permanently coalesced states. We have demonstrated that the persistence of these merged structures reflects the energetic properties of two-dimensional FTSs rather than a transient dynamical effect. In particular, direct energy comparisons show that the bound post-collision core has a lower energy than the sum of the energies of the two separated flat-top solitons before collision, confirming that coalescence is energetically favored. Effective interaction potentials extracted from collision trajectories show that in-phase solitons experience a net attractive interaction that drives strong overlap. The subsequent stability of the merged object is explained by interfacial energetics: a Young-Laplace-type balance between bulk pressure and interfacial line tension provides a natural mechanism for stabilizing the post-collision state. A variational analysis based on direct energy minimization supports this picture. The existence of a robust local minimum in the variational energy landscape explains why, once strong overlap occurs, the system relaxes toward a stable merged configuration rather than fragmenting or dispersing. In this sense, coalescence emerges as a consequence of the combined bulk incompressibility and interfacial energetic cost inherent to two-dimensional FTSs.

Finally, the results reported here highlight the importance of interfacial energetics in higher-dimensional flat-top soliton dynamics. The combined use of collision diagnostics, effective interaction forces, and energetic characterization provides a coherent framework for understanding elastic, inelastic, and coalescent scattering processes. This framework can be extended to explore the role of surface tension in more complex geometries, including anisotropic FTSSs, externally confined systems, non-head-on collision scenarios, and interactions among multiple

solitons in two dimensions.

## ACKNOWLEDGMENTS

M. O. D. Alotaibi acknowledges support from the Kuwait Foundation for the Advancement of Sciences (KFAS) under the KFAS–ICTP Kuwait Programme and the Kuwait Visiting Scientists Scheme Fellowship. L. Al Sakkaf acknowledges support from the ICTP–Arab Fund Associates Programme (ARF01–AFESD Grant No. 14/2023) under the project “Advancing the Capabilities of Arab Researchers and Students”.

---

[1] N. N. Akhmediev and A. Ankiewicz, *Solitons: Nonlinear Pulses and Beams* (Chapman and Hall, London, 1997).

[2] C. Sulem and P. L. Sulem, *The Nonlinear Schrödinger Equation: Self-Focusing and Wave Collapse* (Springer-Verlag, New York, 1999).

[3] Y. S. Kivshar and G. P. Agrawal, *Optical Solitons* (Academic Press, San Diego, 2003).

[4] T. Dauxois and M. Peyrard, *Physics of Solitons* (Cambridge University Press, Cambridge, 2006).

[5] A. Hasegawa and Y. Kodama, *Solitons in Optical Communications* (Oxford University Press, New York, 1995).

[6] G. P. Agrawal, *Nonlinear Fiber Optics*, 3rd ed. (Academic Press, San Diego, 2001).

[7] L. F. Mollenauer and J. P. Gordon, *Solitons in Optical Fibers* (Academic Press, Boston, 2006).

[8] F. Mitschke, *Fiber Optics: Physics and Technology*, 2nd ed. (Springer, 2016).

[9] B. Prinari, J. Nonlinear Math. Phys. **30**, 317 (2023).

[10] M. J. Ablowitz and H. Segur, *Solitons and the Inverse Scattering Transform* (Society for Industrial and Applied Mathematics, Philadelphia, 1981).

[11] Kh. O. Abdulloev, I. L. Bogolubsky, and V. G. Makhankov, Phys. Lett. A **56**, 427 (1976).

[12] P. Cheiney *et al.*, Phys. Rev. Lett. **120**, 135301 (2018).

[13] F. Böttcher *et al.*, Rep. Prog. Phys. **84**, 012403 (2021).

[14] Z. H. Luo *et al.*, Front. Phys. **16**, 32201 (2021).

[15] A. Cappellaro, T. Macrì, G. F. Bertacco, and L. Salasnich, Sci. Rep. **7**, 13358 (2017).

[16] G. Ferioli *et al.*, Phys. Rev. Lett. **122**, 090401 (2019).

[17] V. Cikojević, L. V. Markić, G. E. Astrakharchik, and J. Boronat, Phys. Rev. A **99**, 023618 (2019).

[18] R. Sachdeva, M. N. Tengstrand, and S. M. Reimann, Phys. Rev. A **102**, 043304 (2020).

[19] M. Ota and G. E. Astrakharchik, SciPost Phys. **9**, 020 (2020).

[20] H. Hu and X.-J. Liu, Phys. Rev. Lett. **125**, 195302 (2020).

[21] M. Guo and T. Pfau, Front. Phys. **16**, 32202 (2021).

[22] N. Guebli and A. Boudjemâa, Phys. Rev. A **104**, 023310 (2021).

[23] D. Novoa, H. Michinel, and D. Tommasini, Phys. Rev. Lett. **103**, 023903 (2009).

[24] Y. Li, Z. Chen, Z. Luo, C. Huang, H. Tan, W. Pang, and B. A. Malomed, Phys. Rev. A **98**, 063602 (2018).

[25] U. Al Khawaja, M. O. D. Alotaibi, and L. Al Sakkaf, Phys. Rev. E **110**, 044215 (2024).